Vol. 4(1), pp. 1-17, 2025
eISSN: 2976-4009

ASEAN Journal of Process Control

Research Article

Modeling and Control of CO_2 Capture Plant using Model Predictive Control

Ang Hui Yun[1], Fakhrony Sholahudin Rohman [2,3], Dinie Muhammad [1 *]

[1]Chemical Engineering Department, Faculty of Chemical and Energy Engineering, Universiti Teknologi Malaysia, 81310 Johor Bahru, Johor, Malaysia

[2]Process Systems Engineering Centre (UTM-PROSPECT), Research Institute of Sustainable Environment (RISE), Universiti Teknologi Malaysia, 81310 Johor Bahru, Johor, Malaysia

[3]Faculty of Engineering, Universiti Malaysia Sabah, Jalan UMS, 88450, Kota Kinabalu, Sabah, Malaysia

*Corresponding Author: dinie.muhammad@utm.my

Abstract:

The increasing concentration of atmospheric carbon dioxide (CO_2) necessitates the development of efficient carbon capture technologies to mitigate climate change. Post-combustion capture using Monoethanolamine (MEA) is a mature technology; however, its operational efficiency is hindered by process nonlinearities and multivariable interactions. This research focuses on enhancing the control of a CO_2 absorption column by implementing a Model Predictive Control (MPC) strategy. A dynamic process model was first developed and validated using Aspen Plus Dynamics. Subsequently, a linear state-space model was derived from this high-fidelity model through system identification techniques. The performance of the MPC was then benchmarked against a conventional Proportional-Integral (PI) control scheme in both setpoint tracking and disturbance rejection scenarios. The results demonstrate that the MPC provides superior control, exhibiting faster settling times, minimal overshoot, and more effective disturbance rejection compared to the PI controller. The enhanced performance, quantified by a lower Integral Squared Error (ISE), highlights the capability of MPC to handle complex process dynamics and improve the stability and efficiency of CO_2 capture plants.

Keywords: Carbon Capture; Model Predictive Control; State Space Model; Aspen Plus;

1. Introduction

Global carbon dioxide (CO_2) emissions remain a central challenge for contemporary climate policy and industrial practices. In 2023, global energy-related CO_2 emissions rose by 1.1%, reaching a new record of approximately 37.4 billion tons, underscoring the persistent reliance on fossil fuels and highlighting the critical need for mitigation technologies alongside rapid decarbonization efforts (IEA, 2024). Carbon capture and storage (CCS) has emerged as a vital component of pathways aimed at limiting temperature rise while maintaining industrial and power sector reliability (Mullen et al., 2024). Among various CCS technologies, post-combustion absorption using aqueous amine solvents, such as Monoethanolamine (MEA), remains the most mature and widely studied method for retrofitting existing combustion sources (Vinjarapu et al., 2024). Pilot-scale campaigns have extensively characterized operational performance, mass transfer behavior, and solvent chemistry under realistic flue-gas conditions. These studies highlight both the practical viability of MEA systems and their

principal limitations, particularly the substantial thermal reboiler duty, solvent degradation, and sensitivity to changing flue-gas conditions (Mullen et al., 2024; Rúa et al., 2021).

From an operations and control perspective, solvent-based capture plants are challenging due to their multivariable, tightly coupled nature and susceptibility to measurable and unmeasured disturbances, such as variations in flue-gas flow, composition, and temperature. Traditional single-loop PID or PI structures often struggle to deliver consistent capture efficiency while simultaneously minimizing solvent usage and energy consumption across the full operating envelope (Ilea et al., 2024). Consequently, advanced control strategies have been proposed and tested for capture systems to improve setpoint tracking, disturbance rejection, and process economics in dynamic environments (He et al., 2018; Sultan et al., 2022).

Model Predictive Control (MPC) is particularly appealing for carbon capture applications because it explicitly utilizes a process model to predict future plant behavior, enforces process and output constraints, and optimizes control actions over a finite horizon. The theoretical foundations and demonstrated industrial benefits of MPC in multivariable chemical processes are well established (Sultan et al., 2022). In the specific context of CO_2 capture, earlier studies have shown that model-based strategies can improve solvent management and stabilize capture efficiency under load-following operation and transient disturbances, which are increasingly important as power plants and industrial sites operate flexibly to accommodate variable renewables (Rúa et al., 2021; Wu et al., 2018). Practical deployment of MPC for capture plants typically combines rigorous process simulation (e.g., Aspen Plus/Dynamics) with controller design and validation in MATLAB/Simulink using MPC toolboxes, enabling a workflow that couples detailed steady-state and dynamic representations with controller synthesis and closed-loop testing (Anugraha & Brata, 2023; Decardi-Nelson & Liu, 2022; Ma et al., 2021).

This paper builds on a simulation and control study of a MEA-based post-combustion pilot plant to present a concise evaluation of MPC for absorber control under representative disturbances and operating changes. The work integrates detailed process simulation, system identification for reduced-order linear models, and closed-loop MPC design to evaluate controller performance in comparison to conventional PI strategies. Key contributions of the manuscript are: (1) a validated simulation framework for absorber dynamics suitable for control studies; (2) a systematic selection of manipulated and controlled variables based on sensitivity analysis; and (3) comparative closed-loop results showing MPC benefits in setpoint tracking and disturbance rejection. These results aim to inform both practitioners and researchers about the practical tradeoffs and benefits of deploying MPC in solvent-based CO_2 capture systems, and to identify open challenges for future work.

2. Methodology

This section describes the data sources, process modelling, dynamic surrogate development, system identification procedure, controller design, and the evaluation framework used to compare Model Predictive Control (MPC) with a conventional PI controller. The workflow proceeds from (i) data collection and steady-state modelling, to (ii) dynamic surrogate construction and excitation data generation, (iii) reduced-order model identification, and finally (iv) MPC design, tuning, and closed-loop assessment.

2.1 Process description and data collection

The process and data required to develop a credible simulation were collected from the project documentation by Notz et al. (2012). The baseline operating conditions included flue-gas composition and flow, lean solvent composition and flow, temperatures, pressures, column geometry, and liquid/gas (L/G) ratio. Thermodynamic and kinetic parameters (equilibrium constants, rate constants, and activation energies) relevant to the MEA–CO_2 zwitterion/carbamate chemistry were compiled from the literature (Jana & De, 2014) and pilot-plant records, ensuring that the simulation captured the dominant chemical and transport phenomena.

A brief description of the pilot plant is as follows: flue gas from a natural-gas burner (containing CO_2, O_2, N_2, and water vapor) is conditioned using a blower and a pre-washer (direct-contact cooler) to reach an absorber inlet temperature of ≈approximately 45–50 °C. Flow control is achieved through the use of blower speed, inlet valves, and throttling elements. Online instrumentation provides continuous measurements of flow, pressure, temperature, and gas composition (CO_2, O_2), which were used both for steady-state validation and for disturbance characterization (for example, flue-gas

temperature and composition variability). The CO_2 pilot plant process flow diagram is shown in Figure 2.1.

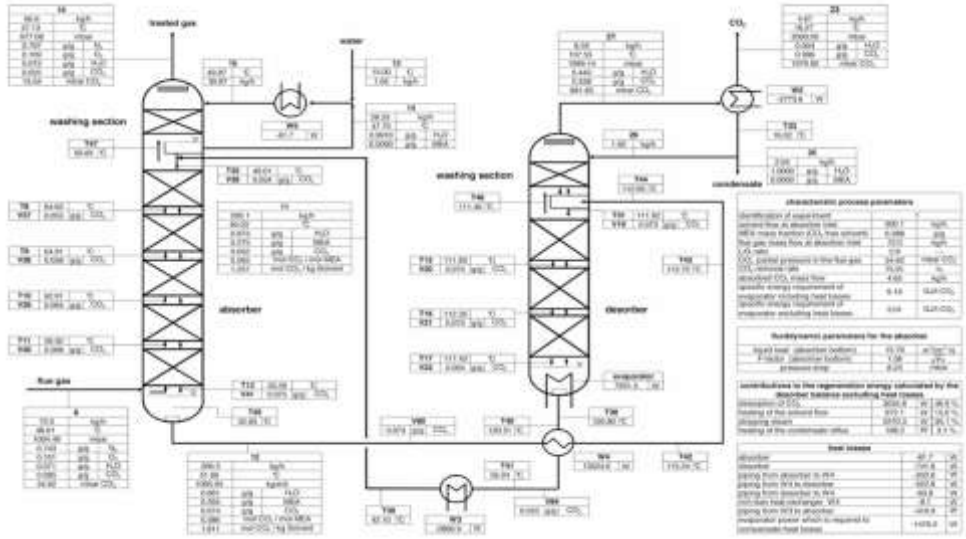

Figure 2.1 Pilot Plant Process Flow Diagram (Notz et al., 2012)

Here are Tables 2.1 and 2.2, which summarize the fundamental data, including operating conditions and reactor sizing, for the plant simulation, as extracted from the PFD diagram of the carbon capture pilot plant.

Table 2.1: Feed Condition and Operating Condition (Notz et al., 2012)

Stream ID	Process Variable	Value
FLUEGAS (Inlet Flue Gas)	Inlet Flue Gas Flow Rate, (kg/h)	72.0
	Mass Fraction of CO_2, (g/g)	0.085
	Mass Fraction of O_2, (g/g)	0.101
	Mass Fraction of N_2, (g/g)	0.743
	Mass Fraction of H_2O, (g/g)	0.071
	Temperature, (°C)	48.01
	Pressure, (mbar)	1004.49
LEANIN (Inlet recycled solvent with low concentration of CO_2)	Flow Rate, (kg/h)	201.3
	Mass Fraction of MEA, (g/g)	0.275
	Mass Fraction of CO_2, (g/g)	0.051
	Mass Fraction of H_2O, (g/g)	0.674
	Molar CO_2 loading	0.254
	Temperature, (°C)	40.01
	Pressure, (mbar)	2000

Note: Mass fraction of MEA in CO_2 free solvent = 0.288

Table 2.2: Specification of Column Design (Notz et al., 2012)

	Height of packing (m)	Internal Diameter, (mm)	Column Pressure, (mbar)
Absorber	4.20	125	1013.2
Desorber	2.52	125	1999.1
L/G Ratio	2.8		

2.2 Chemical reactions and thermodynamic data

In the carbon capture process, the absorption of carbon dioxide (CO_2) by Monoethanolamine (MEA) in an aqueous solution primarily occurs through the formation of carbamate and bicarbonate ions. The main chemical reactions involved are:

(a) Reaction 1: Water Dissociation
$2H_2O \leftrightarrow H_3O^+ + OH^-$
(b) Reaction 2: Carbon Dioxide Dissociation to form Bicarbonate (HCO_3^-)
$2H_2O + CO_2 \leftrightarrow H_3O^+ + HCO_3^-$
(c) Reaction 3: Bicarbonate Dissociation to form Carbonate (CO_3^{2-})
$H_2O + HCO_3^- \leftrightarrow H_3O^+ + CO_3^{2-}$
(d) Reaction 4: Dissociation of Protonated MEA
$H_2O + MEAH^+ \leftrightarrow H_3O^+ + RNH_2$
(e) Reaction 5: Formation of Carbamate ($MEACOO^-$)
$H_3O^+ + MEA \leftrightarrow H_2O + MEACOO^-$

The principal chemical pathways in MEA absorption involve the formation of carbamate and bicarbonate species, as well as related acid–base equilibria, which are represented in the model. Relevant equilibrium expressions were parameterized using the common logarithmic or empirical form used in the literature:

$$\ln K = A + \frac{B}{T} + C \ln T + DT$$

(with T in K and coefficients A, B, C, D taken from Jana and De (2014) work). The chemical kinetics were represented following the zwitterion/carbamate mechanism, in which zwitterion formation (MEA + CO_2 → zwitterion) is commonly the rate-determining step. The absorption rate is typically second-order in the reacting species; the exact kinetic form and parameters employed in the simulation were taken from the cited sources and are reproduced in Table 2.3.

Table 2.3 Equilibrium Constant for Respective Reactions (Jana & De, 2014)

Reaction	A	B	C	D
1	132.89888	-13445.9	-22.477301	0
2	231.4654390	-12092.1	-36.781601	0
3	216.050446	-12431.7	-35.481899	0
4	-3.038325	-7008.3569	0	-0.003135
5	-0.52135	-2545.53	0	0

The zwitterion mechanism describes the reaction between MEA and CO_2, resulting in the formation of carbamate ions ($MEACOO^-$). This mechanism is crucial for understanding the kinetics of CO_2 absorption by MEA and involves two main steps:

(a) Formation of the Zwitterion Intermediate:
$MEA + CO_2 \rightarrow MEA^+COO^-$
(b) Deprotonation of the Zwitterion to Form Carbamate:
$MEA^+COO^- \rightarrow MEA^+COO^-$

The rate-determining step (RDS) in this mechanism is the formation of the zwitterion intermediate ($MEA + CO_2 \rightarrow MEA^+COO^-$), as it controls the overall reaction rate. This step can be affected by factors such as temperature, pressure, and MEA concentration. A second-order rate law expresses the reaction rate for the formation of $MEACOO^-$ via the zwitterion mechanism:

$$RCO_2 = k[MEA][CO_2]$$

$$RCO_2 = \frac{[MEA][CO_2]}{\frac{1}{k_2} + \frac{1}{k_{MEA}[MEA] + k_{H_2O}[H_2O] + k_{OH}[OH^-]}}$$

In this equation, 'k' is the equilibrium constant for the zwitterion intermediate formation, '[MEA]' is the concentration of Monoethanolamine, and '[CO_2]' is the concentration of carbon dioxide. The equilibrium constant 'k' is further influenced by temperature, as described by the Arrhenius Equation: k = A exp(-Ea/RT), where 'A' is the pre-exponential factor, 'Ea' is the activation energy, 'R' is the universal gas constant, and 'T' is the temperature.

2.3 Steady-state simulation and thermodynamic modelling (Aspen Plus)

A detailed steady-state flowsheet of the absorber, stripper, and auxiliary equipment (including heat exchangers, pumps, and reboiler) was implemented in Aspen Plus. Thermophysical and chemical non-idealities in the amine–water–gas system were modelled using the ELECNRTL property method, and where applicable, the Kent–Eisenberg correlation was used for equilibrium behavior. Rate-based RADFRAC/RPLUG blocks, incorporating the zwitterion mechanism, were employed for steady-state rate-based simulations where feasible.

The steady-state model was iteratively adjusted until key outputs (CO_2 capture fraction, rich/lean loadings, outlet partial pressure and heat duties) matched pilot-plant measurements within acceptable error bounds, thereby providing a validated operating point and baseline for subsequent dynamic work. Differences between rate-based and equilibrium solutions were recorded and later used to discuss the limitations of surrogate modelling.

2.4 Dynamic modelling and integration with MATLAB/Simulink

The validated steady-state flowsheet was translated into a dynamic representation in Aspen Dynamics by assigning holdups, time constants and realistic actuator dynamics and by defining control volumes and initial conditions consistent with the steady state. Because full rate-based dynamics are computationally demanding and not always tractable for real-time co-simulation, an equilibrium-based dynamic approximation was adopted when needed to permit robust AMSimulation export and co-simulation with MATLAB/Simulink. The dynamic plant was exported as an AMSimulation block and integrated in Simulink; signal mappings (manipulated inputs, measured outputs, and disturbances) were verified and sampled at the controller sampling interval chosen for identification and control design.

2.5 Sensitivity analysis and control variable selection

A sensitivity analysis guided the choice of manipulated variables (MVs), controlled variables (CVs) and nominally measured disturbances (DVs). The candidate variables were selected from process understanding and instrumentation availability. The final control configuration (presented in Table 2.2) focused on the following:

- Manipulated variables (MVs): flue-gas flow rate (MV1) and lean solvent (MEA) flow rate (MV2), chosen for their direct influence on L/G ratio and CO_2 removal.
- Controlled variables (CVs): CO_2 flow rate at GASOUT (CV1) as a primary performance indicator, MEA flow at RICHOUT (CV2) to reflect solvent circulation and loading, column pressure (CV3) and column temperature (CV4) as stability and kinetics indicators.
- Disturbances (DVs): The flue-gas temperature was treated as the primary measurable disturbance due to its significant impact on CO_2 solubility and reaction rates.

Systematic perturbation experiments in the dynamic model (including step changes and ±10 %, ±20 %, and ±30% variations) were used to quantify effect sizes, settling times, and cross-coupling. Results were ranked by sensitivity and dynamic importance, which motivated a parsimonious 2×2 MPC architecture (two MVs controlling two primary CVs) that balances control authority, observability, and practical actuator limits.

2.5 Data generation and system identification

To obtain control-oriented models, the AMSimulation plant was excited using bounded pseudo-random sequences (uniform random variations within ±30% of nominal, with dwell times sufficient to excite dominant modes) applied to the selected MVs. Output signals were recorded at the controller

sampling interval. The recorded dataset was pre-processed (filtered, detrended, outliers removed, and normalized), then partitioned into estimation and validation sets.

Model identification used MATLAB System Identification Toolbox to estimate reduced-order discrete-time state-space models. The model order was selected based on fit metrics, residual whiteness tests, and frequency-domain agreement. Where identifiability problems arose, the excitation design was refined, and experiments were repeated until a satisfactory tradeoff between fidelity and parsimony was achieved.

2.6 MPC design and tuning

The identified state-space model served as the prediction model for a constrained linear MPC implemented using MATLAB MPC Toolbox. The prediction and control horizons were chosen to capture the dominant modes while maintaining tractable online optimization. The quadratic cost penalized tracking errors and control effort to balance CO_2 removal and actuator usage. Input and rate constraints reflected realistic actuator capabilities. The measured disturbance (flue-gas temperature) was incorporated in the prediction model either as a known exogenous input or via disturbance estimation to achieve offset-free behavior.

Tuning proceeded iteratively in closed-loop simulation: weightings, horizons and constraint tightness were adjusted to obtain acceptable transient responses without violating actuator limits. Robustness was assessed by introducing parametric variations (to represent model uncertainty), unmodeled dynamics, and applying sensitivity scenarios (±10 %, ±20 %, and ±30 % changes). Controller settings were adjusted as necessary to maintain stability and ensure practical MV behavior.

2.8 Performance evaluation and comparison with conventional PI control

The MPC closed-loop performance was compared against a benchmark PI control strategy implemented on the same CV–MV pairing and subject to identical actuator constraints. Test cases included setpoint tracking (for example, ±10% steps) and disturbance rejection (flue-gas temperature perturbations and combined disturbances). Performance metrics included Integral Squared Error (ISE), settling time, overshoot, and cumulative control effort. In addition to control metrics, process-specific indicators (time-averaged CO_2 capture rate, solvent loading excursions, and energy-related quantities, where available) were computed to contextualize controller performance in terms of process economics.

The comparison framework enabled objective conclusions about the practical benefits and tradeoffs of MPC (improved multivariable coordination, constraint handling, and disturbance rejection versus increased computational and tuning effort). The sensitivity of comparative results to the equilibrium surrogate approximation is explicitly addressed in the Results and Discussion section.

3. Results and Discussion

This section reports the validation of the Aspen Plus steady-state model, quantifies the differences between rate-based and equilibrium surrogates used for dynamics, summarizes sensitivity and identification results, and presents the closed-loop comparison between Model Predictive Control (MPC) and a benchmark PI controller. Where relevant, the implications of the equilibrium surrogate approximation (used for dynamic co-simulation) are noted.

3.1 Aspen Plus model simulation

A detailed Aspen Plus model (rate-based steady-state where feasible, ELECNRTL thermodynamics) was constructed for the absorber/stripper flowsheet and compared with pilot-plant data from (Notz et al., 2012). The full CO2 carbon capture plant simulation model is presented in Figure 3.1.

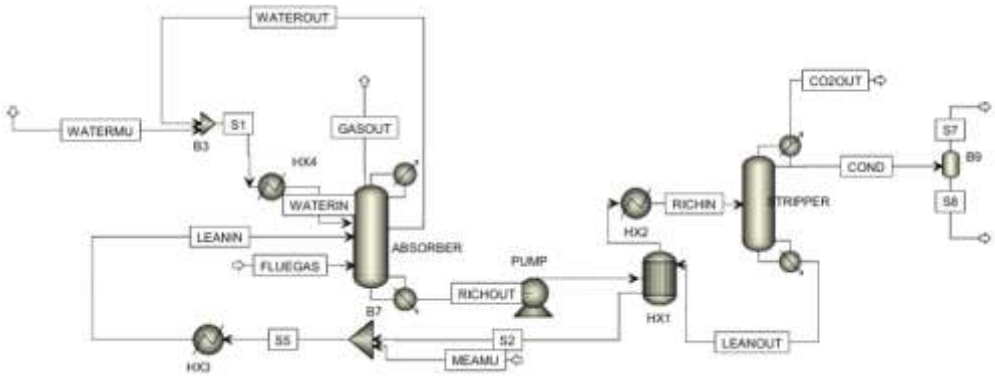

Figure 3.1 CO_2 Capture Plant using Aspen Plus

Table 3.1 summarizes the principal validation metrics used to confirm the steady-state baseline for control studies. Based on the table, the Aspen Plus simulation model reproduces key steady-state outputs within engineering tolerances for control development.

Table 3.1 Steady-state model validation

Output parameter	Experimental (Notz et al., 2012)	Aspen Plus simulation	Error (%)
CO_2 capture (%)	75.910	72.463	4.54
CO_2 loading, RICHOUT (mol CO_2/mol MEA)	0.386	0.365	5.34
CO_2 loading, LEANIN (mol CO_2/mol MEA)	0.265	0.254	4.04
Partial pressure CO_2 at outlet (mbar)	1979.000	1973.635	0.27
Heat exchanger duty (kW)	13.520	12.619	6.66
Stripper reboiler duty (kW)	6.470	7.048	8.93

Figure 3.2 presents the liquid temperature profile along the absorber column. The y-axis represents the liquid temperature (°C), while the x-axis corresponds to the stage number within the absorber. Two datasets are shown for comparison: the Aspen Plus simulation results (solid line) and experimental data reported by Notz (2012) (symbols). The close agreement between the simulated and experimental profiles indicates that the developed model can reliably predict the liquid temperature distribution in the absorber. The validation process confirmed the reliability of the simulation model, with all key metrics falling within acceptable error margins.

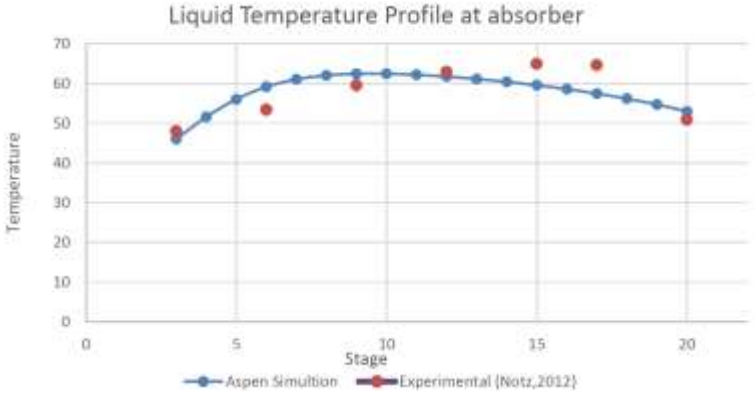

Figure 3.1 Liquid temperature profile along the absorber column

3.2 Rate-based vs Equilibrium-based model

Since a full rate-based dynamic co-simulation could not be exported reliably from Aspen Dynamics, an equilibrium-based dynamic surrogate model was used for closed-loop testing in MATLAB/Simulink. The equilibrium model was chosen because it is simpler, faster to run, and more stable for simulation, even though it does not fully capture mass transfer resistance or kinetic delays that exist in the rate-based model.

In the steady state, the rate-based model predicted a 72.46 per cent capture rate, the equilibrium model predicted 65.16 per cent, while the experimental result was 75.91 per cent, as shown in Table 3.2. This indicates that the equilibrium model underestimates capture performance because it assumes that gas and liquid phases are always in equilibrium, thereby neglecting transport limitations that improve capture in practice. Figure 3.3 shows the absorber column model using rate-based model in the Aspen Dynamic environment.

Table 3.2 CO_2 capture rate: experiment vs rate-based vs equilibrium surrogate

Model Type	CO_2 capture rate (%)
Experiment (Notz et al., 2012)	75.91
Rate-based model	72.46
Equilibrium-based model	65.16

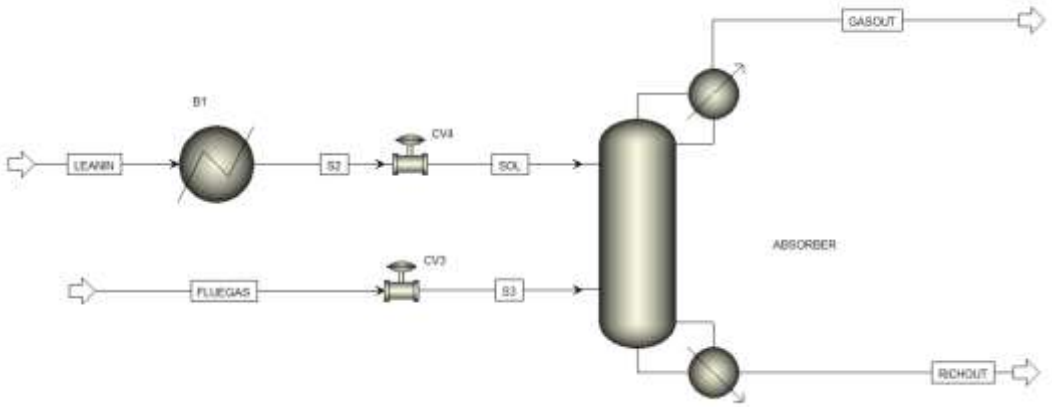

Figure 2.3 Rate-based absorber column model

3.3 Sensitivity analysis results

Systematic perturbations of the process inputs (±10%, ±20%, and ±30%) were carried out to quantify the effect sizes and dynamic behavior associated with two factors: MV1, the flue gas flow rate, and MV2, the lean solvent (MEA) flow rate. The sensitivity analysis revealed that the two manipulated flows have a significant influence on the primary outputs, namely the CO_2 outlet flow CV1 and the MEA-rich flow CV2 and were therefore selected as the principal actuators for the reduced two-by-two MPC configuration.

Figure 3.4 illustrates the dynamic response of the absorber column to step changes in the flue gas flow rate (MV1), which serves as a primary manipulated variable. The results demonstrate a strong, direct, and rapid correlation between the flue gas input and the CO_2 flow rate at the gas outlet (CV1); as the flue gas flow rate increases, more CO_2 exits the column, and vice versa. Simultaneously, the MEA flow rate at the rich outlet (CV2) shows a slower, more gradual response to these changes, indicating the hydraulic lag and mass transfer dynamics within the column. This analysis confirms that the flue gas flow rate has a significant and predictable influence on key process outputs, validating its selection as a principal actuator for the control system.

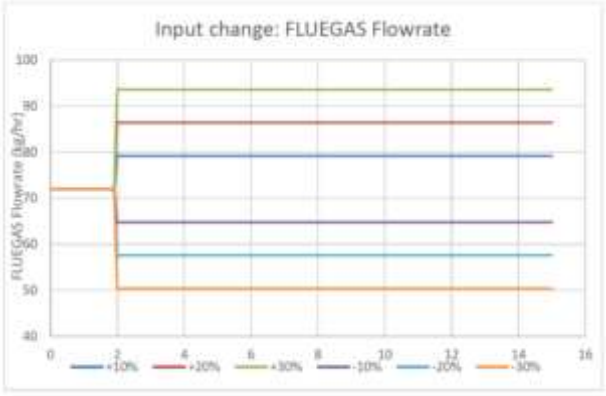

(a)

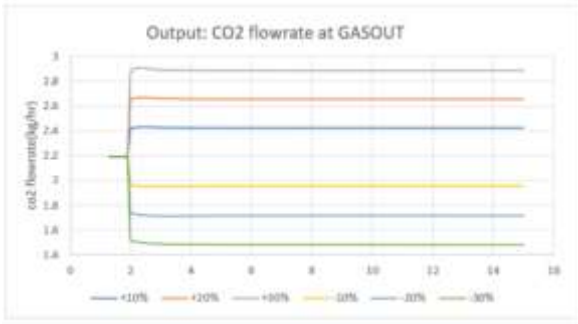

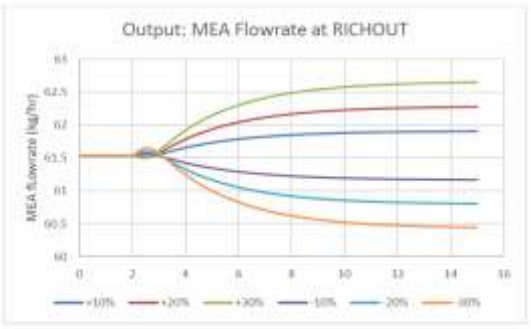

(b) (c)

Figure 3.4 Scenario 1; Effect of Flue gas change as in (a) towards CO_2 flowrate (b) and MEA flowrate

Figure 3.5 presents the system's response to perturbations in the lean MEA solvent flow rate (MV2), the second manipulated variable. The results show a clear inverse relationship between the solvent flow and the CO_2 flow at the outlet (CV1): increasing the lean solvent flow enhances CO_2 absorption, thereby reducing the amount of CO_2 exiting in the treated gas. The dynamic response exhibits a slight overshoot before stabilizing, which is characteristic of the complex interactions between fluid dynamics and reaction kinetics in the absorber. These findings underscore the direct impact of the solvent circulation rate on CO_2 capture efficiency, confirming its crucial role as a manipulated variable for effective process control.

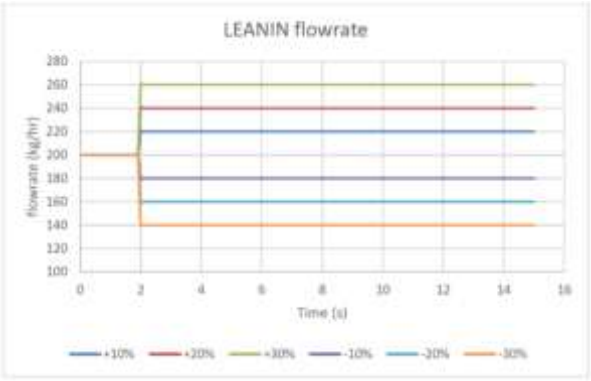

(a)

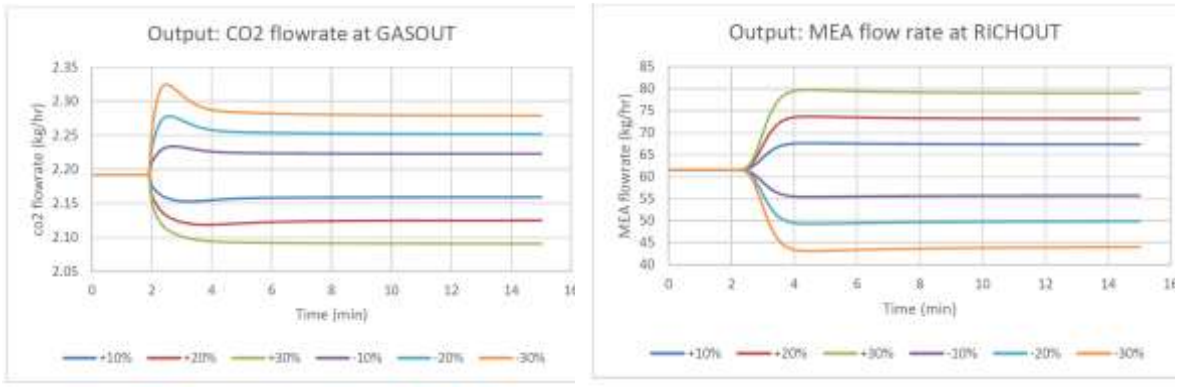

(b) (c)

Figure 3.3 Scenario 2; Effect of Lean (MEA-rich) Gas flow rate changes towards CO_2 flowrate (b) and MEA flowrate

3.4 Data generation and state space model identification

Data for system identification were generated by exciting the AMSimulation plant with uniform random step signals applied to the selected manipulated variables. Excitation amplitudes of up to ±30% about the nominal operating point were employed so that persistence of excitation across the frequency band relevant to absorber–stripper dynamics was ensured. The simulated outputs were sampled at the controller's sampling interval, then pre-processed by detrending, outlier removal, and normalization before being partitioned into estimation and validation subsets. The final identification dataset comprised approximately 20,000 samples and encompassed a wide range of operating conditions intended to expose both fast and slow dynamic modes.

A reduced-order discrete-time state-space model was estimated from the pre-processed data using MATLAB's System Identification Toolbox. Model order selection and parameter estimation were guided by goodness-of-fit criteria, residual whiteness tests and frequency-domain agreement between measured and modelled responses. Where identifiability issues were observed, the excitation design was iteratively refined, and the estimation was repeated until a satisfactory balance between model fidelity and parsimony was achieved. Noise modelling was included to account for measurement disturbances and to avoid overfitting to high-frequency variations that are not relevant for controller design.

The identififed State space model is a discrete-time model with 9 state, 2 inputs, 2 outputs and no direct feedthrough ($D = 0$), with sample time ($T_s = 0.1$) in the standard form:

$$x(t + T_s) = A, x(t) + B, u(t) + K, e(t),$$
$$y(t) = C, x(t) + D, u(t) + e(t)$$

The matrices are shown below and can be used directly to recreate the model in MATLAB (as in sys = idss(A,B,C,D,K,0.1);)

A = [0.9462 -0.07615 0.006743 0.001449 -0.004938 -0.001355 -0.001641 -0.0004728 -0.005349;
0.1466 0.9428 -0.2058 -0.05416 -0.004874 0.01995 9.931e-05 0.001726 0.0006853;
-0.1212 0.27 0.8118 -0.2815 0.009853 0.01888 0.01498 0.006058 -0.006471;
0.1805 -0.007759 0.5137 0.5911 -0.06067 0.1776 0.0925 0.01332 -0.001515;
-0.02977 0.02817 -0.03032 0.1392 0.92 0.1082 0.1376 0.09487 0.1541;
0.09059 -0.1105 0.03724 -0.461 0.08172 0.66 -0.4317 -0.08232 0.2162;
0.1171 -0.1142 0.0663 -0.5117 0.05673 -0.1497 0.6901 -0.2361 0.02335;
-0.05154 0.0236 -0.07888 0.09451 -0.09399 0.3423 0.3147 0.1345 0.1837;
0.01229 -0.003429 0.02205 -0.007526 0.01811 -0.1295 -0.01107 0.02382 0.3804];

B = [5.07e-05 1.153e-06;
0.001999 2.661e-05;
0.002597 0.0001229;

```
    0.004209  -0.0005981;
    0.01262    0.0002737;
    0.005742  -0.001759;
   -0.004918  -0.001019;
   -0.003844   0.002223;
   -0.03173    0.0002571 ];

C = [ -0.5935   0.2536  -0.2187   0.1792   1.311   0.6621  -0.2124  0.03335  0.08173;
      419.4   -16.55    1.69     0.1528   0.5269  0.1053   0.01816 0.003532 0.0118  ];

D = [ 0 0;
      0 0 ];

K = [  0.001228  0.006729;
       0.053     0.03989;
       0.08058   0.1065;
       0.1721    0.1734;
       0.3476   -0.08967;
      -0.1054   -0.5706;
      -0.3357   -0.1313;
      -0.5249   -0.9929;
      -0.5804   -0.4912 ];
```

Validation of the identified model was performed on the held-out dataset and assessed quantitatively and qualitatively. The best validation fits obtained were 84.01% for CV1 (CO_2 flow rate at GASOUT) and 98.98% for CV2 (MEA flow rate at RICHOUT) as shown in Figure 3.6. The very high fit for CV2 indicates that the surrogate and identification procedure capture internal solvent circulation dynamics with high fidelity. In contrast, the lower fit for CV1 suggests the presence of residual unmodeled dynamics, most likely associated with flue-gas temperature disturbances and simplified representation of gas-phase mass transfer in the equilibrium surrogate.

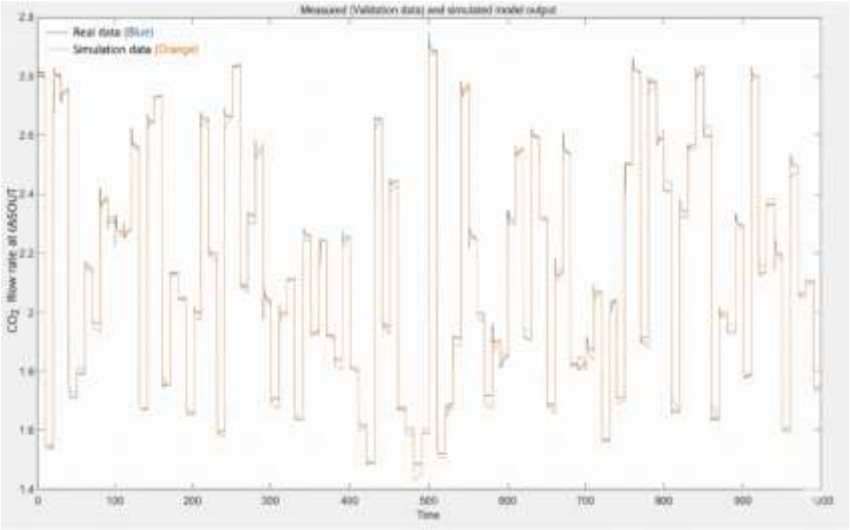

(a)

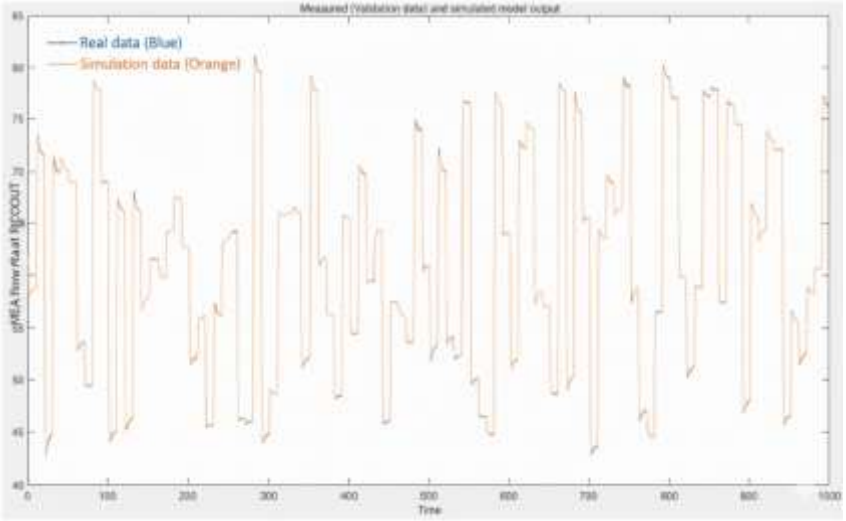

(b)

Figure 3.4 Model Validation profile for CV1 (a) and CV2 (b)

3.5 Closed-loop controller performance

To evaluate its effectiveness in controlling the CO_2 absorption process, the developed Model Predictive Control (MPC) controller was rigorously compared against a Proportional-Integral (PI) controller. The selection of a PI controller over a Proportional-Integral-Derivative (PID) controller was justified explicitly by the nature of the manipulated variables (MV1 and MV2), which are flow rates. For flow control applications in industrial processes, PI controllers are generally favored because derivative action is highly susceptible to noise prevalent in flow measurements, which can potentially lead to excessive control actions and instability. Conversely, flow control dynamics often approximate first-order processes, for which PI control is deemed sufficient to achieve stable and responsive performance.

The comparative assessment between MPC and PI controllers was based on two principal performance criteria: setpoint tracking and disturbance rejection. While MPC possesses inherent advantages in managing multivariable interactions and constraints, PI control remains widely utilized due to its simplicity, ease of tuning, and computational efficiency. Here, a disturbance model is developed to study the effect of changes in flue gas temperature on CV1 (CO_2) and CV2 (MEA). This model is developed using relationships derived from both input-output behavior and simulation data. Based on the relationship, a lookup table is used in the MATLAB Simulink to represent the relationship. Figure 3.7 and 3.8 present the control scheme using State Space MPC and PI controller for CCU absorber column control.

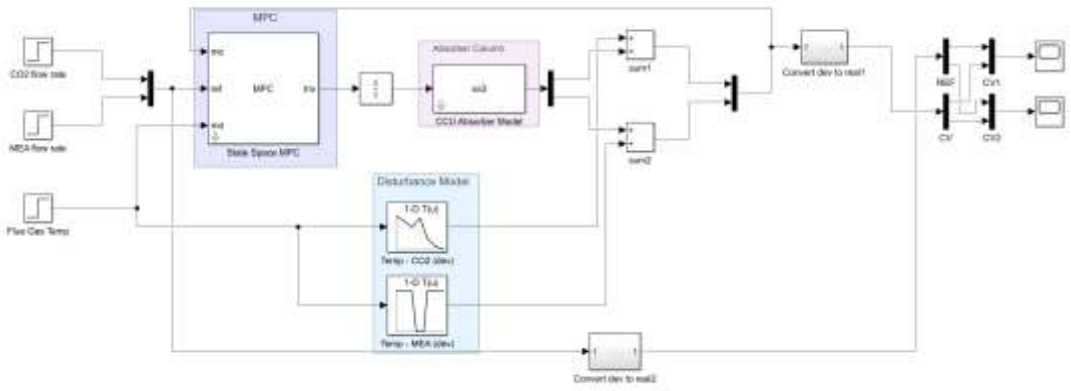

Figure 3.5 CO_2 Capture Absorption column control scheme using MPC

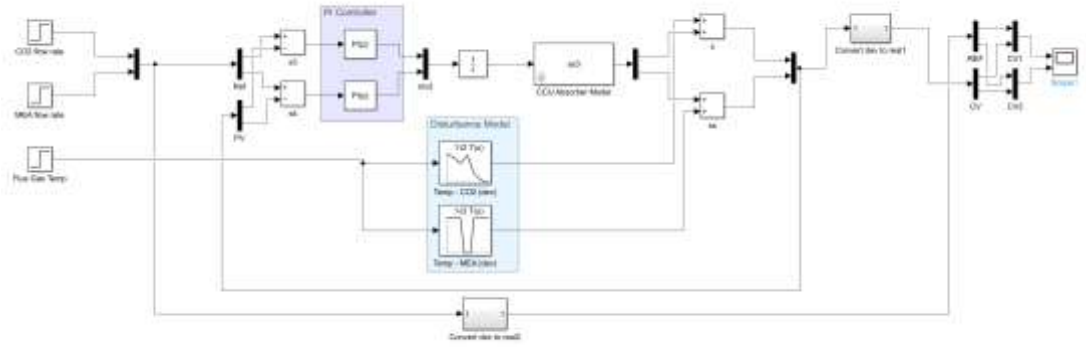

Figure 3.6 CO_2 Capture Absorption column control scheme using PI control

3.5.1 Controller Tuning

The Model Predictive Controller (MPC) was designed in MATLAB's MPC Designer with a prediction horizon of 11, control horizon of 2, and tuning rate weights of 0.1 for both control inputs. This setup provides a balance between fast response and robustness, avoiding overly aggressive control actions. The MPC tuning aimed to achieve stable closed-loop performance while maintaining good disturbance rejection. In comparison, the two PID controllers were tuned using MATLAB's PID Tuner, with K_p = 0.63 and K_i = 12.69 for PID 1 and K_p = 0.07 and K_i = 1.43 for PID 2. These values show that PID 1 provides a faster and more responsive action, while PID 2 is tuned for a slower, smoother response.

3.5.2 Setpoint Tracking

Based on Figure 3.9, in the CV1 subplot(a), the Model Predictive Controller is seen to reach the new reference more quickly and with a smaller steady-state error than the PI controller, because the prediction model and corrective action, anticipated to meet the future plant behavior, were scheduled accordingly. Here, CV1 represents the CO_2 flow rate at GASOUT, and MV1 represents the flue gas flow rate. When the setpoint change was applied, the MPC computed a prompt increase in MV1 to steer the gas composition and flow toward the target, while simultaneously accounting for actuator limits and expected future disturbances. By contrast, the PI controller reacted to the error only after it appeared, so the MV1 command followed a slower, smoother ramp, and the output took longer to settle. The slower PI response is compounded by gas-phase and mass transfer dynamics, which introduce lag and make purely reactive control less effective. The MPC ability to exploit a dynamic model, therefore, produces a faster, lower-error transient at the expense of a larger initial actuator excursion.

Moreover, in the CV2 subplot(b), the same pattern is observed, but the underlying physical reasons differ slightly. CV2 is the MEA flow rate at RICHOUT, and MV2 is the lean solvent (MEA) flow rate. The solvent circulation dynamics were captured with high fidelity in the identified model, so the MPC predictive adjustments of MV2 drove CV2 rapidly toward the new reference with reduced transient deviation. The MPC initial MV2 correction was relatively large and then relaxed as the solver optimized the control effort and adhered to the constraints. The PI controller, lacking prediction, relied on incremental integral action and therefore produced a gentler MV2 ramp and a slower approach to steady state. Additionally, because solvent flow adjustments couple to gas-phase behavior in the column, the MPC coordinated multivariable moves reduced interaction effects more effectively than the single-loop PI, improving transient performance for CV2. In both cases, the tradeoff between faster tracking and larger initial actuator activity is apparent and must be considered in relation to actuator capability and process wear in a practical implementation.

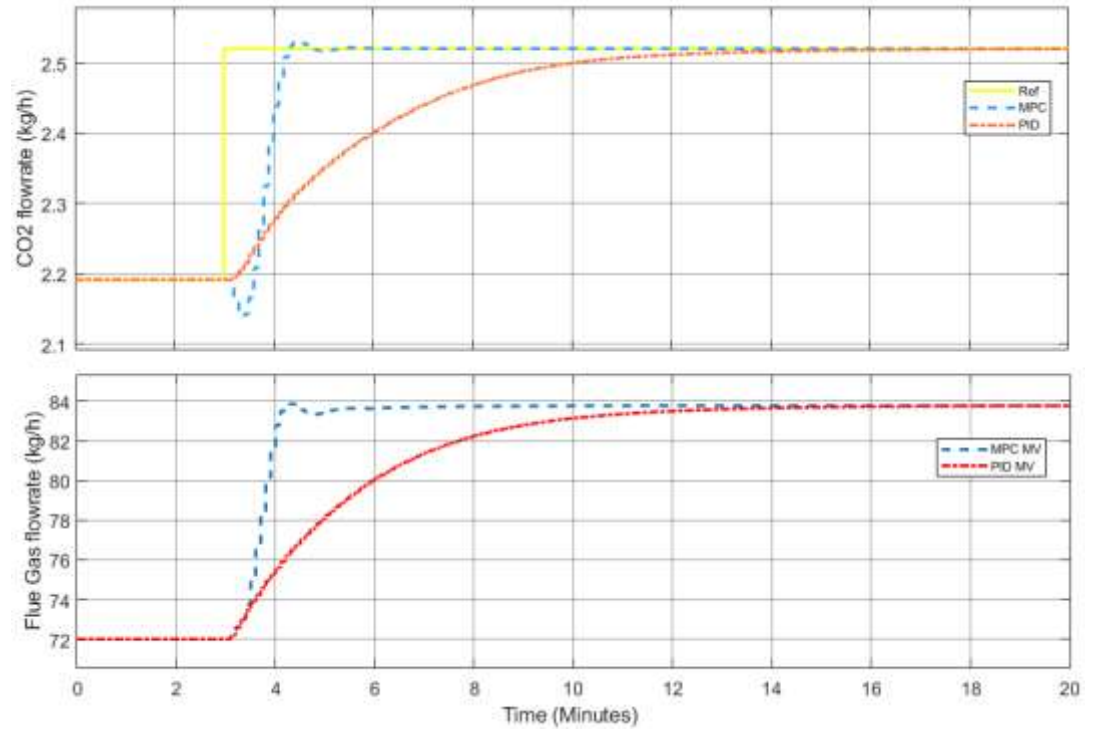

(a)

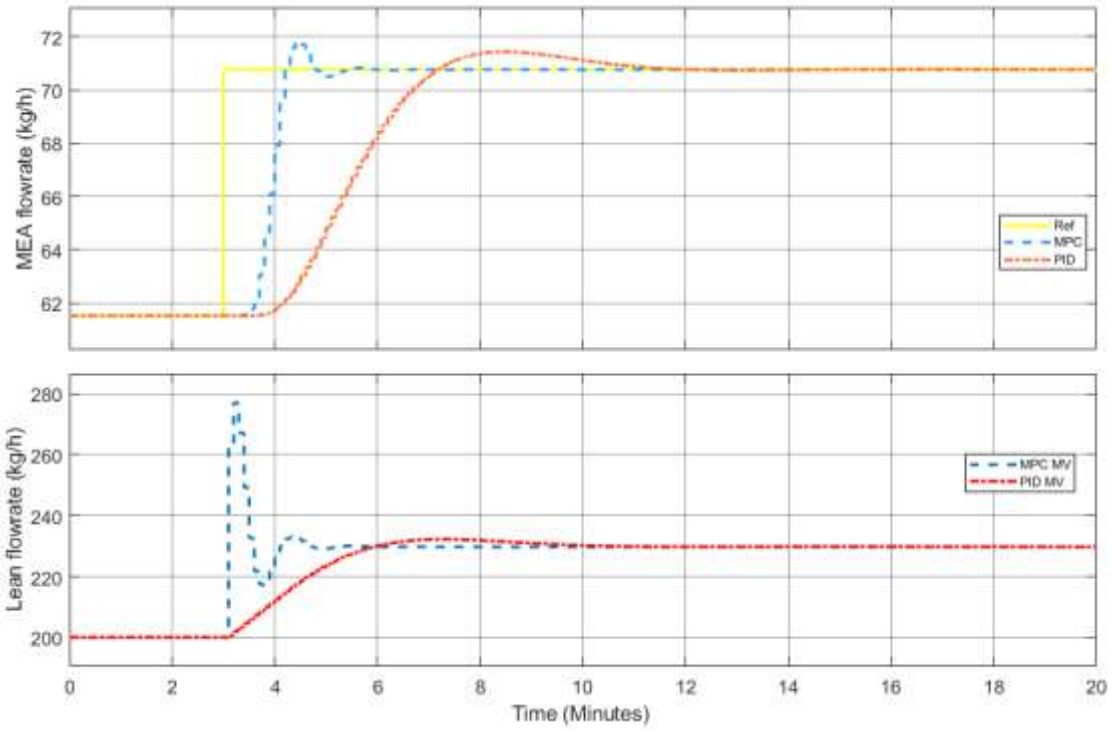

(b)

Figure 3.7 Setpoint tracking performance results and MV profile for CV1 (a) and CV2 (b)

3.5.3 Disturbance Rejection

Based on Figure 3.10, in the CV1 subplot(a), the disturbance response is shown for the CO_2 flow rate at GASOUT, with MV1 being the flue gas flow rate. When the disturbance occurred, the MPC produced a prompt corrective action, which is evident as a sharp excursion in MV1 and a rapid transient in the CV1 trace. This initial predictive correction drove the output back toward the reference faster than the PI controller, which responded more gradually and therefore exhibited a larger and more prolonged deviation before settling. The prominent MPC spike in the manipulated variable is consistent with anticipatory compensation applied by the predictive controller when disturbance information or disturbance estimates are available. The PI behavior is typical of a reactive controller that must first

accumulate error before producing substantial corrective action. In practice, the MPC advantage is a faster return to setpoint and a minor sustained error at the cost of a larger short-term actuator movement.

Besides, in the CV2 subplot(b), the disturbance effect on the MEA flow at RICHOUT and the corresponding MV2 profile are shown. The MPC again effected a quicker corrective change in MV2, resulting in a faster reduction of the disturbance-induced deviation in CV2 relative to the PI controller. The PI action followed with a smoother but slower change in MV2 and a slower approach to steady state. Because the identified model well captured solvent flow dynamics, the predictive controller was able to coordinate the multivariable response more effectively and to reduce interaction effects that might otherwise prolong recovery. As in the CV1 case, the superior disturbance attenuation achieved by MPC was obtained at the expense of more decisive initial actuator motion, which must be evaluated against actuator limits and operational robustness in a real installation.

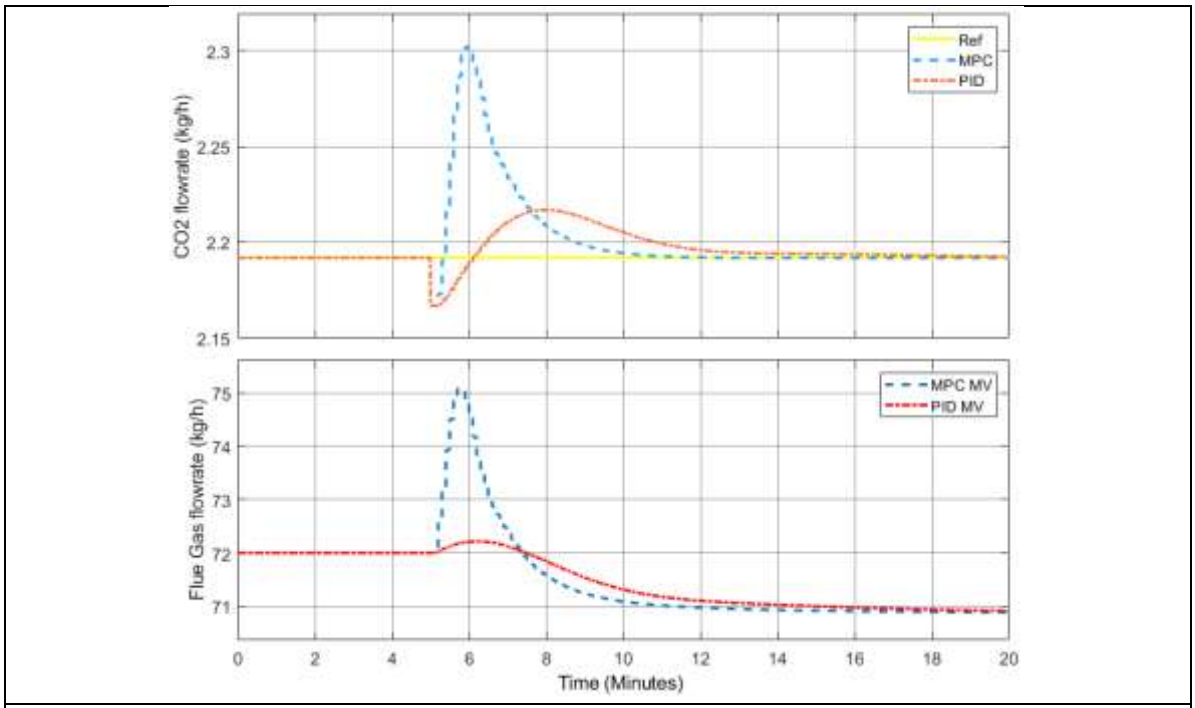

(a)

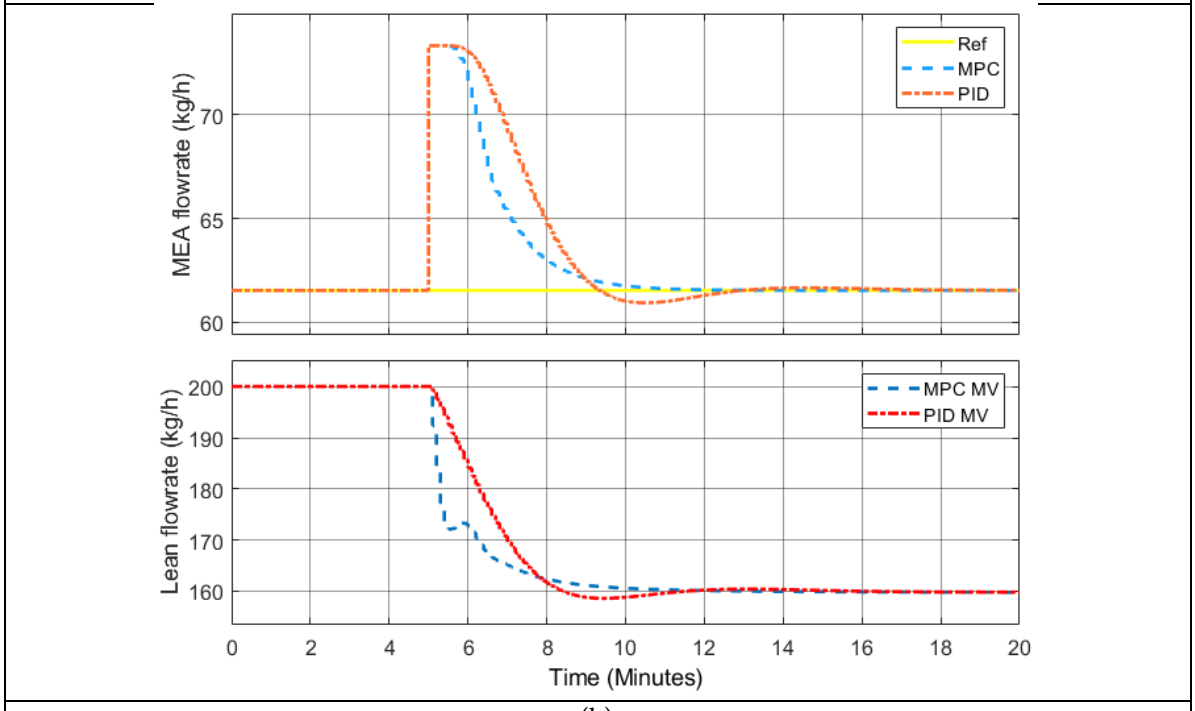

(b)

Figure 3.8 Disturbance rejection performance results and MV profile for CV1 (a) and CV2 (b)

3.5.4 Results summary

Table 3.3 indicates that MPC produces substantially better setpoint performance for both controlled variables. For CV1, the integrated squared error (ISE) decreases from 0.170 under PI control to 0.098 with MPC, representing a reduction of approximately 42%. For CV2, the ISE is reduced from 168 to 71, corresponding to a reduction of approximately 58%. For the disturbance tests, the results are mixed: CV1 shows a lower ISE under PI (0.002) than under MPC (0.011), whereas CV2 shows improved disturbance performance with MPC, where the ISE decreases from 276 under PI to 189 under MPC (about 31 per cent improvement).

These differences can be explained by model fidelity and the nature of the process dynamics. The identified model fit for CV2 was very high, at approximately 98.98%, indicating that MPC predictions and optimization were reliable, and both setpoint and disturbance performance improved significantly. By contrast, CV1 was fitted less well, at approximately 84.01%, and is strongly influenced by gas-phase mass transfer and temperature dynamics that are not fully represented by the equilibrium surrogate and the prediction model. Under the specific disturbance used, the PI controller was able to reject the perturbation more effectively, likely because it was tuned to respond to that disturbance shape, and because MPC was limited by model mismatch and its weightings. To mitigate this imbalance, the prediction model should explicitly include flue gas temperature or utilize disturbance estimation, and the MPC weights should be adjusted to enable more decisive disturbance rejection when necessary.

Table 3.3 Comparison of MPC and PI control performance

Controllers	ISE for Setpoint Tracking Test (+10% from steady state)		ISE for Disturbance Rejection Test (-10% from steady state)	
	CV1	CV2	CV1	CV2
MPC	0.098	71	0.011	189
PI	0.170	168	0.002	276

4. Conclusions

In this study, Model Predictive Control (MPC) was successfully applied to the CO2 capture process using Monoethanolamine (MEA) as the solvent. The simulation results, validation, sensitivity analysis, and performance tests all demonstrate that MPC significantly enhances the performance of the process in terms of setpoint tracking, disturbance rejection, and overall system stability. The MPC controller outperformed the traditional PI controller in all metrics, demonstrating its effectiveness for multivariable control problems in industrial applications, such as CO2 capture. The findings provide valuable insights into the application of advanced control strategies for enhancing CO_2 capture efficiency and promoting sustainable industrial practices.

Acknowledgments: The authors would like to thank Universiti Teknologi Malaysia for its financial assistance under the UTM Potential Academic Staff (UTM-PAS) Grant with Vote Number Q.J130000.2746.04K48.

References

Anugraha, R. P., & Brata, B. K. (2023). Model Predictive Control for Efficient Process Control: A Case Study for Absorber-Stripper System with MEA in Hydrogen Plant. *ASEAN Journal of Process Control*, *2*(1), 1-13.

Decardi-Nelson, B., & Liu, J. (2022). Robust Economic MPC of the Absorption Column in Post-Combustion Carbon Capture through Zone Tracking. *Energies*, *15*(3), 1140. https://www.mdpi.com/1996-1073/15/3/1140

He, X., Wang, Y., Bhattacharyya, D., Lima, F. V., & Turton, R. (2018). Dynamic modeling and advanced control of post-combustion CO2 capture plants. *Chemical Engineering Research and Design*, *131*, 430-439. https://doi.org/https://doi.org/10.1016/j.cherd.2017.12.020

IEA. (2024). *CO2 Emissions in 2023*. Retrieved 1/8/2025 from https://www.iea.org/reports/co2-emissions-in-2023

Ilea, F.-M., Cormos, A.-M., Cristea, V. M., & Cormos, C.-C. (2024). Hybrid Advanced Control Strategy for Post-Combustion Carbon Capture Plant by Integrating PI and Model-Based Approaches. *Energies*, *17*(12), 2886.

Jana, K., & De, S. (2014). Biomass integrated combined power plant with post combustion CO2 capture–performance study by ASPEN Plus®. *Energy Procedia*, *54*, 166-176.

Ma, C., Zhang, W., Zheng, Y., & An, A. (2021). Economic Model Predictive Control for Post-Combustion CO2 Capture System Based on MEA. *Energies*, *14*(23), 8160. https://www.mdpi.com/1996-1073/14/23/8160

Mullen, D., Braakhuis, L., Knuutila, H. K., Gibbins, J., & Lucquiaud, M. (2024). Monoethanolamine degradation rates in post-combustion CO2 capture plants with the capture of 100% of the added CO2. *Industrial & Engineering Chemistry Research*, *63*(31), 13677-13691.

Notz, R., Mangalapally, H. P., & Hasse, H. (2012). Post combustion CO2 capture by reactive absorption: Pilot plant description and results of systematic studies with MEA. *International Journal of Greenhouse Gas Control*, *6*, 84-112.

Rúa, J., Hillestad, M., & Nord, L. O. (2021). Model predictive control for combined cycles integrated with CO2 capture plants. *Computers & Chemical Engineering*, *146*, 107217. https://doi.org/https://doi.org/10.1016/j.compchemeng.2020.107217

Sultan, T., Zabiri, H., Shahbaz, M., & Maulud, A. S. (2022). Model Analysis for the Implementation of a Fast Model Predictive Control Scheme on the Absorption/Stripping CO2 Capture Plants. *ACS omega*, *7*(10), 8437-8455.

Vinjarapu, S. H. B., Neerup, R., Larsen, A. H., Jørsboe, J. K., Villadsen, S. N. B., Jensen, S., Karlsson, J. L., Kappel, J., Lassen, H., & Blinksbjerg, P. (2024). Results from pilot-scale CO2 capture testing using 30 wt% MEA at a Waste-to-Energy facility: Optimization through parametric analysis. *Applied Energy*, *355*, 122193.

Wu, X., Shen, J., Li, Y., Wang, M., & Lawal, A. (2018). Flexible operation of post-combustion solvent-based carbon capture for coal-fired power plants using multi-model predictive control: A simulation study. *Fuel*, *220*, 931-941.